journal

J. Am. Ceram. Soc., 1–6 (2012)
DOI: 10.1111/j.1551-2916.2012.05085.x

Synthesis and Size Control of Tetragonal Barium Titanate Nanopowders by Facile Solvothermal Method

Hyun-Wook Lee,[‡] San Moon,[‡] Chang-Hak Choi,[§] and Do Kyung Kim[*,†,‡]

[‡]Department of Materials Science and Engineering, Korea Advanced Institute of Science and Technology (KAIST), Daejeon 305-701, Korea

[§]LCR Material Development Group, Samsung Electro-Mechanics, Suwon 443-743, Korea

A facile synthetic strategy was implemented to obtain nanosized barium titanate ($BaTiO_3$) powders with tetragonal structure. The nanoparticles were synthesized using solvothermal process employing diethanolamine and triethanolamine to suppress the particle growth and the as-prepared nanopowders were characterized using X-ray diffraction, scanning electron microscopy, and high-resolution dispersive Raman spectroscopy. It was found that the particle size can be easily tuned by adjusting the experimental parameters while retaining the tetragonality. The average diameters of the particles prepared with and without the organic amines were found to be 80 and 100 nm, respectively. All the synthesized $BaTiO_3$ nanopowders exhibit a narrow size distribution with a uniform morphology. Rietveld refinement of the XRD patterns and Raman spectra revealed that the synthesized $BaTiO_3$ nanopowders have tetragonal asymmetry dominant structures. A slight decrease in the tetragonality of the prepared powders with decrease in particle size is attributed to the presence of cubic shell layer and inner defects. The tetragonal-dominant structure was also confirmed by normalizing the peak area of the Raman spectra.

I. Introduction

BARIUM titanate ($BaTiO_3$) has been utilized extensively in various electroceramic areas, including thermistors,[1] electroluminescence,[2] electro-optical devices,[3–5] and multilayer ceramic capacitors (MLCC)[6,7] due to its ferroelectric response and high dielectric constant.[8,9] As technological advances demand more complex portable devices with various functions, the fabrication of thinner dielectric layers of MLCCs becomes a more significant issue as these devices becomes more miniaturized. This requires reduction in $BaTiO_3$ particle size to nanoscale dimensions.

As the sizes of $BaTiO_3$ particles decrease below 100 nm, the formidable challenge related to the fabrication of miniaturized MLCCs lies in the gradual decline in the dielectricity of the layers.[10] It is well known that $BaTiO_3$ exists in several polymorphic phases, such as tetragonal and cubic structures with ferroelectric and paraelectric features, respectively. In tetragonal $BaTiO_3$, a structural deformation due to the displacement of the Ti atom from the octahedron center causes the ferroelectric stabilization of tetragonal $BaTiO_3$.[11] However, nanosized $BaTiO_3$ reduces the spontaneous polarization of Ti atoms at the surface region, resulting in a cubic shell layer. Consequently, the main challenges lie in the synthesis of highly dielectric $BaTiO_3$ nanopowders with decrease in particle size. Moreover, various defects can exist inside the particles, such as oxygen vacancies[12] and lattice impurities.[13,14] Therefore, to downsize the dielectric layers in MLCCs further, thinner cubic shell layers and a method that reduces the number of defects inside the $BaTiO_3$ nanopowders should be considered to acquire the highest possible dielectricity.

Another issue pertaining to $BaTiO_3$ nanopowders involves controlling the particle size distribution. Conventional solid-state synthesis can yield larger quantities, but it is difficult to achieve a narrow particle size distribution when the particle sizes are less than 100 nm. Particle dispersity affects the fabrication of MLCCs when using tape-casting and sintering processes. Nonuniform particle sizes can lead to vacancies inside $BaTiO_3$ dielectric layers and abnormal grain growth after tape-casting and sintering. In this regard, various soft chemistry techniques have been explored to prepare $BaTiO_3$ nanoparticles, such as spraying[15] and electrophoretic deposition[16,17] as well as the catecholate,[18] sol–gel,[19–21] pyrolysis,[22] hydrothermal synthesis using gel powders,[23] and supercritical hydrothermal reaction methods.[24] Although uniform $BaTiO_3$ nanopowders are obtained using these methods, synthetic procedures are generally complex and expensive. Also, these nanoparticles exhibit cubic structure instead of required tetragonal structure, which makes them unsuitable for miniaturized MLCC applications. Hence, a facile and cost-effective method is highly recommended to fabricate fine tetragonal $BaTiO_3$ nanopowders to meet current demands.

In this article, we report the preparation of $BaTiO_3$ nanopowders via hydrothermal and solvothermal synthesis methods and describe their structural characteristics. To control the particle size, organic solvents of diethanolamine (DEA) and triethanolamine (TEA) were employed as part of a solvothermal reaction. The resulting $BaTiO_3$ structure and morphology were characterized using X-ray diffraction, scanning electron microscopy, and Raman spectroscopy to confirm the tetragonal phase and particle size with narrow dispersity. Rietveld refinement of the XRD patterns and Raman spectroscopy were carried out to evaluate the tetragonality of the nanopowders. The results showed that the particle size could be tuned simply by adjusting the experimental parameters. The average sizes of particles prepared with and without DEA and TEA were found to be 80 and 100 nm, respectively.

II. Experimental Procedure

The synthesis of $BaTiO_3$ nanopowders was based on a solvothermal process using barium hydroxide monohydrate ($Ba(OH)_2 \cdot H_2O$ (Ba-hydroxide), 98%, Aldrich, Milwaukee, WI) and titanium butoxide ($Ti[O(CH_2)_3 \cdot CH_3]_4$ (Ti-butoxide), 97%, Aldrich) as starting materials. In a typical $BaTiO_3$ nanopowder fabrication procedure, 17.018 g (50 mmol) of Ti-

S.-J. Kang—contributing editor

Manuscript No. 30582. Received October 31, 2011; approved January 06, 2012.
*Member, The American Ceramic Society.
This study was presented at the International Conference on Sintering 2011, Jeju, Korea, August 29, 2011 (Electroceramics I, Presentation No. MoC 1-1).
†Author to whom correspondence should be addressed. e-mail: dkkim@kaist.ac.kr

butoxide was mixed with 20 mL of high-purity ethanol, after which 7 mL of ammonium hydroxide solution (25% NH_3 in H_2O, Aldrich) was added to the solution mixture. A quantity of 14.204 g (75 mmol) of Ba-hydroxide was dissolved in 25 mL of preheated DI-water to prepare clear Ba-hydroxide solution in parallel. The aqueous Ba-hydroxide solution was then added to the solution mixture. To control the particle size, 5 mL of DEA ($HN(CH_2CH_2OH)_2$, $\geq$98%, Aldrich) or TEA ($(HOCH_2CH_2)_3N$, $\geq$98%, Aldrich) was added to the solution mixture. The final suspension was transferred into a 100 mL Teflon-lined stainless-steel autoclave and heat-treated at 200°C for 48 h. After the reaction, the resultant product was washed repeatedly using water and high-purity ethanol and then dried at 80°C for 24 h in an oven. Also, $BaTiO_3$ nanoparticles were prepared without organic amines as a control sample using similar procedure.

The structural characteristics and phase purity of the synthesized $BaTiO_3$ nanopowders were investigated using an X-ray diffractometer (XRD; Rigaku D/Max-RB (12 kW), Tokyo, Japan) with CuK_α radiation (λ = 1.5418 Å) operating at 40 kV and 100 mA. The unit cell parameters were obtained via Rietveld refinement of the XRD data. The morphology of the nanopowders was observed using a field-emission scanning electron microscope (FE-SEM; Hitachi S-4800, Tokyo, Japan) and a field-emission transmission electron microscope (FE-TEM; Tecnai G² F30 S-Twin, Eindhoven, the Netherlands). The Raman spectra were recorded by a high-resolution dispersive Raman microscope (LabRAM HR UV/Vis/NIR, Horiba Jobin Yvon, Longjumeau, France) equipped with three laser sources (UV, Vis, and NIR), a confocal microscope, and a liquid-nitrogen-cooled charge-coupled device (CCD) multichannel detector (256 pixels × 1024 pixels). The measurements were performed using a 514.5 nm line of an argon ion laser at room temperature. A 50× objective lens was used, and the acquisition time for each Raman spectrum was approximately 10 min depending on the sample. The measured Raman shift was in the range 100–1000 cm^{-1}.

III. Results and Discussion

The as-synthesized $BaTiO_3$ nanopowders were characterized using XRD and SEM. Figure 1 shows the XRD pattern, a SEM image, and the particle size histogram of the hydrothermally synthesized nanopowders, in which organic amines were not added. The XRD pattern indicates that the synthesized material shows good agreement with the conventional tetragonal $BaTiO_3$ structure with the *P*4mm space group (JCPDS data No. 05-0626), with no impurity peak appearing in the diffractogram. Rietveld refinement gives lattice parameters a = 3.99454 Å and c = 4.02411 Å, which are very close to the reported values pertaining to this tetragonal structure (JCPDS data No. 05-0626). XRD pattern of as-synthesized $BaTiO_3$ powders show peak splitting at 45°. In general, the XRD patterns of the tetragonal $BaTiO_3$ show split peaks at 45° corresponding to the (*hkl*) Miller index (002) and (200), whereas cubic $BaTiO_3$ (JCPDS data No. 31-0174) has one single peak at 45° corresponding to (002). Therefore, we can conclude that the hydrothermally synthesized $BaTiO_3$ powders show a tetragonal- or tetragonal-dominant structure. The SEM image confirms that the $BaTiO_3$ powders have a nonagglomerated shape with an average diameter of 106.69 nm. The particle-size distribution histogram in Fig. 1(c) shows that the nanopowders have narrow size distribution ranges with the average particle dispersity (D_{SEM99}/D_{SEM50}) of 1.57. The structural and morphological characterizations converge in demonstrating that the hydrothermal synthesis process leads to the formation of the tetragonal $BaTiO_3$ phase with 100-nm grade nanopowders and a narrow size distribution.

In comparison, the $BaTiO_3$ nanopowders synthesized using the solvothermal process show differences both in terms of

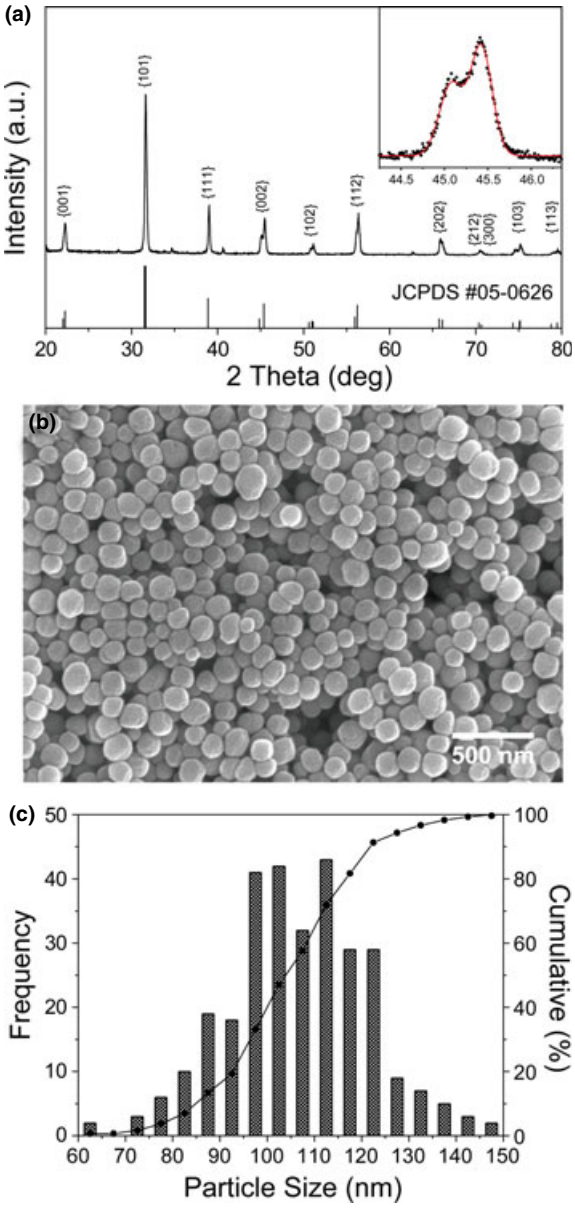

Fig. 1. (a) XRD pattern, (b) typical SEM image, and (c) particle size distribution histogram of hydrothermally synthesized $BaTiO_3$ nanopowders.

the particle size and tetragonality. The XRD patterns of the as-synthesized $BaTiO_3$ created by means of the DEA and TEA processes are shown in Fig. 2. Both patterns indicate a tetragonal $BaTiO_3$ structure with no impurity peak. However, evidence of peak splitting at 45° is not very distinct. This may be due to the peak broadening effect of nano-crystalline structures or to the cubic-dominant $BaTiO_3$ structure. The tetragonalities of the two samples as determined by Rietveld refinement were 1.0068 (DEA) and 1.0072 (TEA). These values are comparable to the tetragonality of nanopowders synthesized using a hydrothermal process. To compare the particle size, the morphologies of $BaTiO_3$ nanopowders created using the DEA and TEA processes were characterized by SEM. These results are presented in Fig. 3. The average sizes (D_{SEM50}) of the two powders are 78.72 nm (DEA) and 84.78 nm (TEA). Micrograph images of the nanopowders revealed particle size reductions of 24.3% (DEA) and 18.5% (TEA) compared with a hydrothermally synthesized sample. Thus, organic amines serve to reduce the particle size of synthesized $BaTiO_3$ nanopowders while retaining their tetragonality.

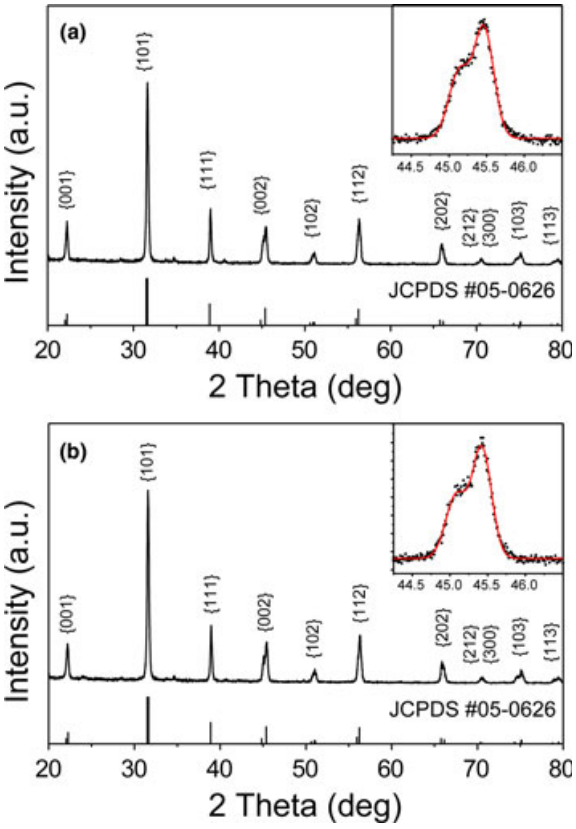

Fig. 2. XRD patterns of $BaTiO_3$ nanopowders synthesized by addition of organic solvents of (a) DEA and (b) TEA.

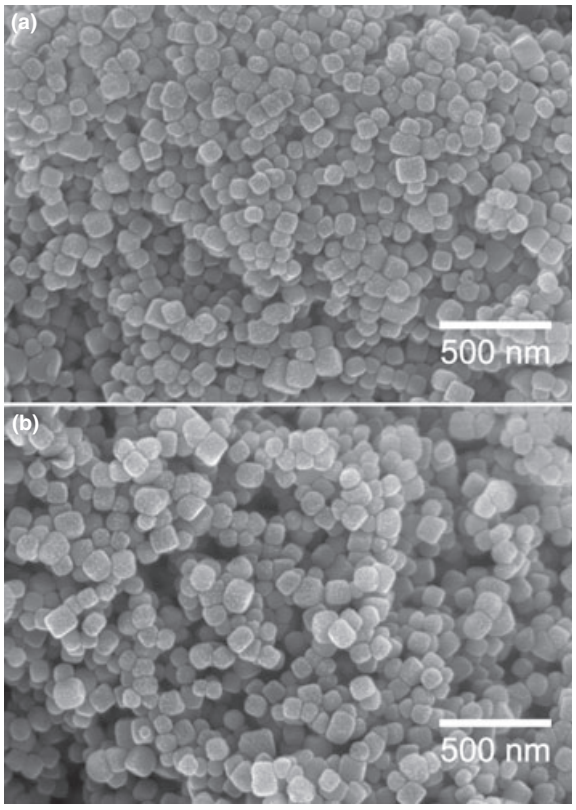

Fig. 3. SEM images of $BaTiO_3$ nanopowders prepared by addition of organic solvents of (a) DEA and (b) TEA.

The tetragonality values determined by Rietveld refinement of the XRD data are difficult to assign the crystal symmetry due to the peak broadening effect and low intensity.

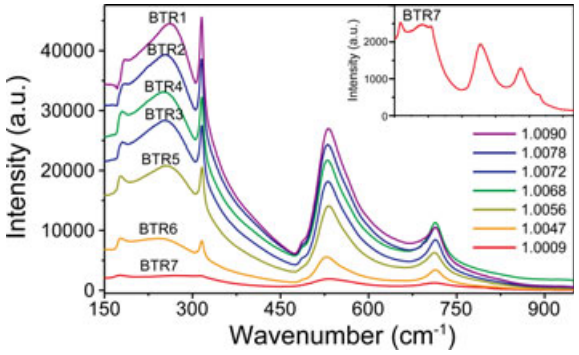

Fig. 4. Plot showing dependence of Raman spectra on tetragonality of $BaTiO_3$ nanopowders.

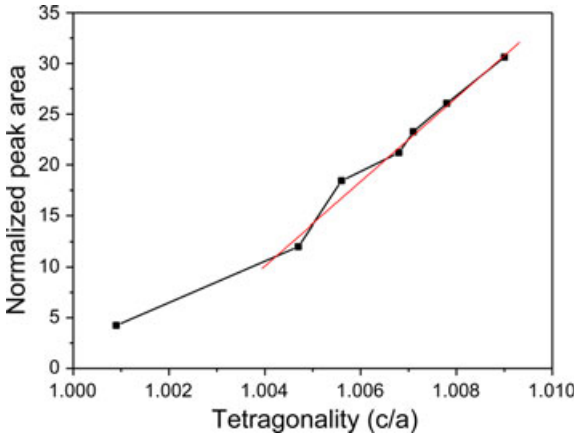

Fig. 5. Correlation between the normalized peak area from the Raman spectra in Fig. 4 and tetragonality determined from XRD data.

Therefore, an alternate analysis method is required to confirm the tetragonalities of $BaTiO_3$ nanopowders. Raman spectroscopy is capable of measuring the lattice vibrational spectra in an investigation of the tetragonal-cubic symmetry of $BaTiO_3$ samples.[25,26] The Raman spectra of different $BaTiO_3$ particles (denoted by BTR1 to BTR7 based on tetragonality) are given in Fig. 4 and their corresponding size, lattice parameters, and tetragonality values are given in Table I. The Raman spectra of BTR1 to BTR6 samples, which have a tetragonal feature according to the XRD data, are consistent with the spectrum of tetragonal $BaTiO_3$ as reported elsewhere.[26,27] It is known that tetragonal $BaTiO_3$ has Raman scattering bands of A_1(TO) at 250 cm^{-1}, B_1, E (TO + LO) at 307 cm^{-1}, [E(TO), A_1(LO)] at 520 cm^{-1}, and [E(LO), A_1(LO)] at 720 cm^{-1}. However, a mixture of the Raman scattering characteristics of both cubic and tetragonal asymmetry can be observed at around 180, 307, 520, and 720 cm^{-1}. In the present experiment, the scattering intensities at 250 and 307 cm^{-1} gradually declined as the tetragonalities of the $BaTiO_3$ nanopowders decreased. It is interesting to note that there is a relationship between the peak intensity and the tetragonal features in the Raman scattering results. Figure 5 demonstrates the tetragonality of $BaTiO_3$ nanopowders as a function of the normalized area of peaks at 180, 250, 307, 520, and 720 cm^{-1}. The normalized peak areas are in very good agreement with the tetragonalities determined by the Rietveld refinement of the XRD data. These results indicate that Raman spectroscopy can serve as an alternate tool with which to evaluate nanosized $BaTiO_3$.

To enhance our understanding of the roles of the organic solvents of DEA and TEA, the amount of DEA was varied

in the experimental procedure. Table II presents a comparison of the particle size, distributions, and lattice parameters of various $BaTiO_3$ nanopowders synthesized using hydrothermal and solvothermal processes by varying the DEA content. The notation of the sample numbers indicates the different ratios of organic solvents and the addition of ethanol. When we added DEA of 2 (BT 4) or 10 mL (BT 5) to the solvothermal reaction, the average particle size decreased by 20%–30% compared with hydrothermally synthesized $BaTiO_3$ (BT 1). Although the volume ratio of organic amines was increased or decreased by 12.5% (BT 5) or 2.5% (BT 3), the particle size decreased in a similar manner by about 75 or 80 nm. Although the DEA process decreased the average particle size, the influence of the amount of DEA on the particle size was insignificant, whereas a reduction in the average size did not occur in BT 6 or 7 despite the addition of DEA. This phenomenon can be explained based on the kinetics of the reaction in relation to ethanol and DEA.[28,29] During the solvothermal reaction, Ti-O bonds are broken via hydrolytic attack to form hydroxytitanium complexes ($Ti(OH)_x^{(4-x)+}$), which are soluble and react further with barium ions or complexes (Ba^{2+} or $BaOH^+$) in a solution.[30] In the present study, ethanol is a solvent with weaker polarity than water; thus, the formation of $Ti(OH)_x^{(4-x)+}$ can occur at a significantly faster rate. Simultaneously, DEA plays a role in the formation of hydrogen bonds with hydrated water of barium salts and exhibits a strong inclination to take Ba^{2+} or $BaOH^+$ away from the hydroxide complexes. This process using DEA is advantageous, as more rapid formation of $Ti(OH)_x^{(4-x)+}$ and the strong attraction with Ba^{2+} or $BaOH^+$ can lead to an increase in the number of nucleation sites and can suppress the particle growth by means of the dissolution-precipitation reaction mechanism.[30] This phenomenon requires both DEA and ethanol to suppress the growth reaction, otherwise a size reduction does not occur, as in the case of the BT 8 sample. Accordingly, with organic amines of DEA and TEA, smaller $BaTiO_3$ particles with a uniform size distribution can be synthesized than hydrothermally synthesized samples.

The theoretical tetragonal asymmetry of $BaTiO_3$ is 1.011 (a = 3.992 Å, c = 4.036 Å), but in the present nanoparticles, the tetragonalities are generally about 1.006 or 1.007. It is known that $BaTiO_3$ nanoparticles contain two general defects[14] attributable to the reduction in the tetragonality of the nanoparticles. The first defect is the presence of a cubic shell layer in $BaTiO_3$.[31,32] In a bulk system, a cubic shell layer with a thickness of a few nanometers is essentially negligible, whereas in nano-sized particles, a few nanometers become a relatively critical value, decreasing the tetragonality of the nanopowders. In addition, hydrothermally synthesized $BaTiO_3$ contains some degree of internal pores due to the presence of OH^- groups in the $BaTiO_3$ nanopowders.[14] These two defects can be presented as a model, as shown in Fig. 6(a). The presence of an outer shell and inner pores in our synthesized $BaTiO_3$ nanopowders were confirmed using scanning transmission electron microscopy (STEM), as shown in Fig. 6(b). Similarly, Zhu *et al.* has observed the outer shell of $BaTiO_3$ nanocrystals by HR-TEM.[32] Therefore, the shell layer and inner pores inevitably influenced the tetragonality of the $BaTiO_3$ nanopowder.

Based on the $BaTiO_3$ model and on the HR-TEM observations by Zhu *et al.*,[32] if the cubic shell layer is assumed to have a thickness of 3 nm thick and if inner defects do not exist in the nanoparticles, the tetragonality as a function of the particle size is plotted as a solid line, as shown in Fig. 7. The calculated line was assumed that the nanoparticle pertain as spheral morphology. There is a drastic decrease in the tetragonality value, from 1.009 to 1.008, when the particle size is less than 80 nm. These values indicate that at an average particle size of 80 nm, the maximum attainable tetragonality of $BaTiO_3$ nanopowders is 1.0087. In a comparison with our synthesized results, all of the tetragonal asymmetry values of the synthesized $BaTiO_3$ nanopowders are presented in Fig. 7. The tetragonality values of BT 1 to 8 are plotted with the white circles, and the black circles represent those values of the reproduced $BaTiO_3$ nanopowders. The tetragonality values of our data show very good agreement with their fitting line (dashed line) and show a declining trend according to the decrease in the particle size. As a result, the tetragonal decline can likely be attributed to the increase in the ratio of the outer cubic shell layer in the $BaTiO_3$ nanopowders, which assumes a more critical value at a smaller

Table I. Average Particle Size, Lattice Parameter, and Tetragonality of $BaTiO_3$ Nanopowders for Raman Spectroscopy

Sample no.	Average particle size† (nm)	a (Å)	c (Å)	Tetragonality‡ (c/a)
BTR1	115.42	3.99375	4.02962	1.0090
BTR2	158.57	3.99009	4.02428	1.0086
BTR3	84.78	3.99435	4.02275	1.0072
BTR4	74.65	3.99260	4.01701	1.0061
BTR5	97.98	3.99849	4.02100	1.0056
BTR6	74.39	3.99721	4.01890	1.0054
BTR7	36.69	4.02867	4.03245	1.0009

†Average particle sizes of BTRs were measured using SEM images (D_{SEM50}).
‡Tetragonalities (c/a) of BTRs were calculated by Rietveld refinement of X-ray diffraction data.

Table II. Comparison of Average Particle Size, Particle Dispersity, and Lattice Parameter of $BaTiO_3$ Nanopowders Produced from Hydrothermal and Solvothermal Reactions

Sample no.	Amine	Amount of amine (mL)	Ethanol	Average particle size† (nm)	Standard deviation (nm)	Particle dispersity (D_{SEM99}/D_{SEM50})	a (Å)	c (Å)	Tetragonality‡ (c/a)	Reference
BT1	X	0	X	106.69	14.69	1.57	3.99454	4.02411	1.0074	Fig. 1
BT2	DEA	5	O	78.72	10.78	1.43	3.99129	4.01824	1.0068	Figs. 2(a) and 3(a)
BT3	TEA	5	O	84.78	11.07	1.42	3.99435	4.02275	1.0072	Figs. 2(b) and 3(b)
BT4	DEA	2	O	81.24	13.58	1.50	3.99792	4.02411	1.0066	–
BT5	DEA	10	O	76.76	17.69	1.75	4.00002	4.02439	1.0061	–
BT6	DEA	5	X	103.97	15.16	1.39	3.98999	4.02018	1.0076	–
BT7	DEA	10	X	103.72	15.55	1.41	3.98818	4.01920	1.0078	–
BT8	X	0	O	101.97	19.23	1.52	3.99333	4.01765	1.0061	–

X, not included; O, included; DEA, diethanolamine ($HN(CH_2CH_2OH)_2$); TEA, triethanolamine ($(HOCH_2CH_2)_3N$).
†Average particle sizes of BTs were measured by SEM images (D_{SEM50}).
‡Tetragonalities (c/a) of BTs were calculated by Rietveld refinement of X-ray diffraction data.

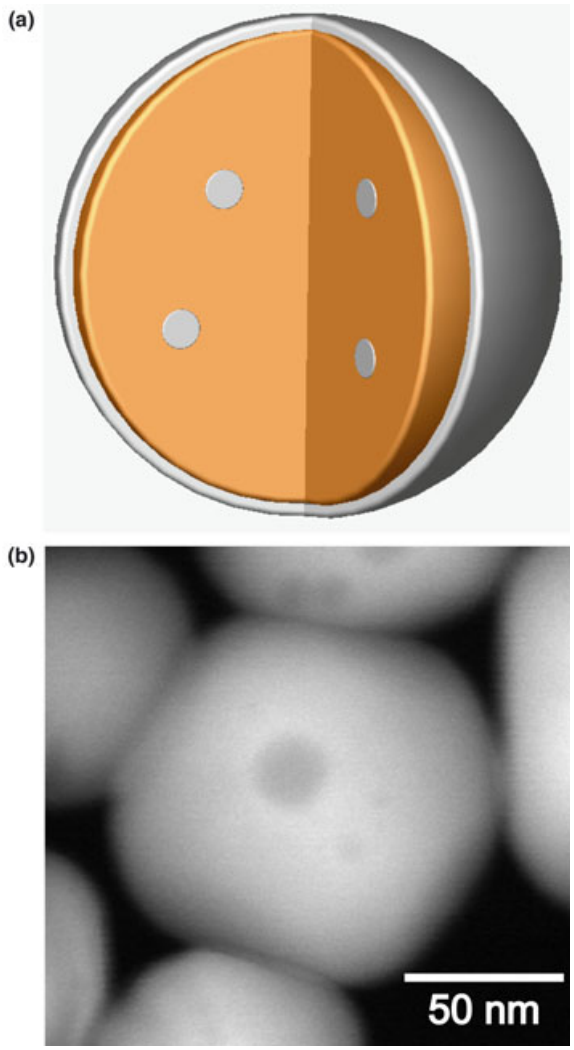

Fig. 6. (a) Schematic representation of a typical $BaTiO_3$ particle. The outer shell layer and inner pores are suggested as a cubic phase. (b) STEM image of as-synthesized $BaTiO_3$ nanopowders.

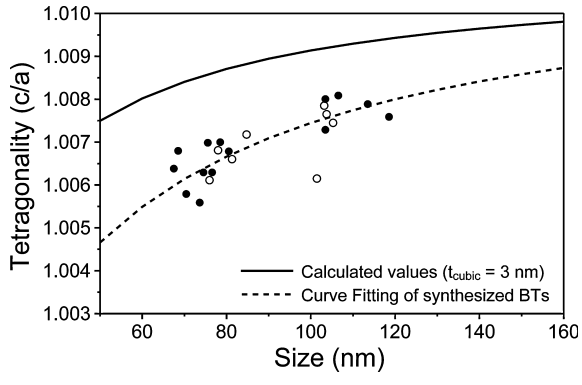

Fig. 7. The fitting plots of tetragonality as a function of particle size generated by diverse synthesized data. Both the curve fitting lines are derived by assuming a simple spheral two-phase model; surface cubic layer and bulk tetragonal phases, in which c/a ratios are 1.000 and 1.011, respectively. The white circles (○) represent the data of BT samples from Table II, and the black circles (●) represent the values of the $BaTiO_3$ nanopowders from different batches.

size. Moreover, the difference between the line of the calculated value and the fitting line may have been attributed to the presence of inner defects.

IV. Conclusion

Tetragonal $BaTiO_3$ nanopowders of two different sizes were fabricated using facile and scalable hydrothermal and solvothermal methods. The average diameters of the $BaTiO_3$ particles obtained using hydrothermal and solvothermal reaction methods were around 100 and 80 nm, respectively, with a low particle dispersity (D_{SEM99}/D_{SEM50}) of approximately 1.5. The reduction in particle size can be attributed to the synergistic effect of organic amine and ethanol in increasing the number of nucleation sites and suppressing the particle growth via dissolution-precipitation mechanism. The tetragonalities of the synthesized powders, as determined by Rietveld refinement of the XRD data and by high-resolution dispersive Raman spectra, decrease with the decrease in particle size. It was revealed that the reduced tetragonality features of $BaTiO_3$ nanopowders are caused by the presence of a cubic shell layer and inner pores, the effects of which become relatively critical in nanosized materials. Also, by measuring the normalized peak areas of the Raman spectra, we established a trend according to the tetragonality values of the $BaTiO_3$. These synthesized $BaTiO_3$ nanoparticles with tetragonal structure could be potentially used for the miniaturization of MLCC devices.

Acknowledgments

The work was supported by the Center for Advanced MLCC Manufacturing Processes of Samsung Electro-Mechanics, the Priority Research Centers Program (2009-0094041), and Program to Solve Climate Changes through the National Research Foundation of Korea (NRF) funded by the Ministry of Education, Science and Technology (MEST) (NRF-2010-C1AAA001-2010-0029031).

References

[1]Y. Luo and X. Liu, "High Temperature NTC $BaTiO_3$-Based Ceramic Resistors," *Mater. Lett.*, **59** [29–30] 3881–4 (2005).
[2]X. Wang, C.-N. Xu, H. Yamada, K. Nishikubo, and X.-G. Zheng, "Electro-Mechano-Optical Conversions in Pr^{3+}-Doped $BaTiO_3$-$CaTiO_3$ Ceramics," *Adv. Mater.*, **17** [10] 1254–8 (2005).
[3]J. Feinberg, D. Heiman, A. R. Tanguay Jr., and R. W. Hellwarth, "Photorefractive Effects and Light-Induced Charge Migration in Barium Titanate," *J. Appl. Phys.*, **51** [3] 1297–305 (1980).
[4]J. O. White, M. Cronin-Golomb, B. Fischer, and A. Yariv, "Coherent Oscillation by Self-Induced Gratings in the Photorefractive Crystal $BaTiO_3$," *Appl. Phys. Lett.*, **40** [6] 450–2 (1982).
[5]X. Y. Meng, Z. Z. Wang, and C. Chen, "Mechanism of the Electro-Optic Effect in $BaTiO_3$," *Chem. Phys. Lett.*, **411** [4–6] 357–60 (2005).
[6]P. K. Singh, S. Cochrane, W.-. T. Liu, K. Chen, D. B. Knorr, J. M. Borrego, E. J. Rymaszewski, and T.-M. Lu, "High-Frequency Response of Capacitors Fabricated from Fine Grain $BaTiO_3$ Thin Films," *Appl. Phys. Lett.*, **66** [26] 3683–5 (1995).
[7]T. M. Shaw, S. Trolier-McKinstry, and P. C. McIntyre, "The Properties of Ferroelectric Films at Small Dimensions," *Annu. Rev. Mater. Sci.*, **30**, 263–298 (2000).
[8]B. Matthias and A. von Hippel, "Domain Structure and Dielectric Response of Barium Titanate Single Crystals," *Phys. Rev.*, **73** [11] 1378–84 (1948).
[9]W. J. Merz, "The Electric and Optical Behavior of $BaTiO_3$ Single-Domain Crystals," *Phys. Rev.*, **76** [8] 1221–5 (1949).
[10]F.-S. Yen, H.-I. Hsiang, and Y.-H. Chang, "Cubic to Tetragonal Phase Transformation of Ultrafine $BaTiO_3$ Crystallites at Room Temperature," *Jpn. J. Appl. Phys.*, **34** [11] 6149–55 (1995).
[11]D. Hennings, "Barium Titanate Based Ceramic Materials for Dielectric Use," *Int. J. High Technol. Ceram.*, **3** [2] 91–111 (1987).
[12]R. D. Levi and Y. Tsur, "The Effect of Oxygen Vacancies in the Early Stages of $BaTiO_3$ Nanopowder Sintering," *Adv. Mater.*, **17** [13] 1606–8 (2005).
[13]E. Ciftci, M. N. Rahaman, and M. Shumsky, "Hydrothermal Precipitation and Characterization of Nanocrystalline $BaTiO_3$ Particles," *J. Mater. Sci.*, **36** [20] 4875–82 (2001).
[14]L. Qi, B. I. Lee, P. Badheka, L.-Q. Wang, P. Gilmour, W. D. Samuels, and G. J. Exarhos, "Low-Temperature Paraelectric-Ferroelectric Phase Transformation in Hydrothermal $BaTiO_3$ Particles," *Mater. Lett.*, **59** [22] 2794–8 (2005).
[15]K. K. Lee, Y. C. Kang, K. Y. Jung, and J. H. Kim, "Preparation of Nano-Sized $BaTiO_3$ Particle by Citric Acid-Assisted Spray Pyrolysis," *J. Alloys Compd.*, **395** [1–2] 280–5 (2005).
[16]J. Li, Y. J. Wu, H. Tanaka, T. Yamamoto, and M. Kuwabara, "Preparation of a Monodispersed Suspension of Barium Titanate Nanoparticles and Electrophoretic Deposition of Thin Films," *J. Am. Ceram. Soc.*, **87** [8] 1578–81 (2004).

[17]T. Hosokura, Y. Sakabe, and M. Kuwabara, "Preparation of Barium Titanate with Patterned Microstructure by a Novel Electrophoretic Deposition Method," *J. Sol-Gel. Sci. Technol.*, **33** [2] 221–8 (2005).

[18]W. Maison, R. Kleeberg, R. B. Heimann, and S. Phanichphant, "Phase Content, Tetragonality, and Crystallite Size of Nanoscaled Barium Titanate Synthesized by the Catecholate Process: Effect of Calcination Temperature," *J. Eur. Ceram. Soc*, **23** [1] 127–32 (2003).

[19]M. H. Frey and D. A. Payne, "Synthesis and Processing of Barium Titanate Ceramics from Alkoxide Solutions and Monolithic Gels," *Chem. Mater.*, **7** [1] 123–9 (1995).

[20]S. O'Brien, L. Brus, and C. B. Murray, "Synthesis of Monodisperse Nanoparticles of Barium Titanate: Toward a Generalized Strategy of Oxide Nanoparticle Synthesis," *J. Am. Chem. Soc.*, **123** [48] 12085–6 (2001).

[21]R. L. Brutchey and D. E. Morse, "Template-Free, Low-Temperature Synthesis of Crystalline Barium Titanate Nanoparticles Under Bio-Inspired Conditions," *Angew. Chem. Int. Ed.*, **45** [39] 6564–6 (2006).

[22]P. R. Arya, P. Jha, and A. K. Ganguli, "Synthesis, Characterization and Dielectric Properties of Nanometer-Sized Barium Strontium Titanates Prepared by the Polymeric Citrate Precursor Method," *J. Mater. Chem.*, **13** [2] 415–23 (2003).

[23]J. Y. Choi, C. H. Kim, and D. K. Kim, "Hydrothermal Synthesis of Spherical Perovskite Oxide Powders Using Spherical Gel Powders," *J. Am. Ceram. Soc.*, **81** [5] 1353–6 (1998).

[24]K. Matsui, T. Noguchi, N. M. Islam, Y. Hakuta, and H. Hayashi, "Rapid Synthesis of $BaTiO_3$ Nanoparticles in Supercritical Water by Continuous Hydrothermal Flow Reaction System," *J. Cryst. Growth*, **310** [10] 2584–9 (2008).

[25]C. H. Perry and D. B. Hall, "Temperature Dependence of the Raman Spectrum of $BaTiO_3$," *Phys. Rev. Lett.*, **15** [17] 700–2 (1965).

[26]R. Asiaie, W. Zhu, S. A. Akbar, and P. K. Dutta, "Characterization of Submicron Particles of Tetragonal $BaTiO_3$," *Chem. Mater.*, **8** [1] 226–34 (1996).

[27]Y. Shiratori, C. Pithan, J. Dornseiffer, and R. Waser, "Raman Scattering Studies on Nanocrystalline $BaTiO_3$ Part I – Isolated Particles and Aggregates," *J. Raman Spectrosc.*, **38** [10] 1288–99 (2007).

[28]P. Muralidharan, S. H. Jo, and D. K. Kim, "Electrical Conductivity of Submicrometer Gadolinia-Doped Ceria Sintered at 1000°C Using Precipitation-Synthesized Nanocrystalline Powders," *J. Am. Ceram. Soc.*, **91** [10] 3267–74 (2008).

[29]S. H. Jo, P. Muralidharan, and D. K. Kim, "Low-Temperature Sintering of Dense Lanthanum Silicate Electrolytes with Apatite-Type Structure Using an Organic Precipitant Synthesized Nanopowder," *J. Mater. Res.*, **24**[1] 237–44 (2009).

[30]J. O. Eckert Jr., C. C. Hung-Houston, B. L. Gersten, M. M. Lencka, and R. E. Riman, "Kinetics and Mechanisms of Hydrothermal Synthesis of Barium Titanate," *J. Am. Ceram. Soc.*, **79** [11] 2929–39 (1996).

[31]S. Wada, T. Hoshina, K. Takizawa, M. Ohishi, H. Yasuno, H. Kakemoto, and T. Tsurumi, "Origin of Ultrahigh Dielectric Constants for Barium Titanate Nanoparticles," *J. Kor. Phys. Soc.*, **51** [2] 878–81 (2007).

[32]X. Zhu, Z. Zhang, J. Zhu, S. Zhou, and Z. Liu, "Morphology and Atomic-Scale Surface Structure of Barium Titanate Nanocrystals Formed at Hydrothermal Conditions," *J. Cryst. Growth*, **311** [8] 2437–42 (2009). □